Supporting Information

Catalytic Acceptorless Dehydrogenation of Amines with Ru($P^R_2N^{R'}_2$) and Ru(dppp) Complexes

*James M. Stubbs, Richard J. Hazlehurst, Paul D. Boyle, and Johanna M. Blacquiere**

Department of Chemistry
University of Western Ontario
London, Ontario, Canada, N6A 5B7

Table of Contents

I – NMR Spectra

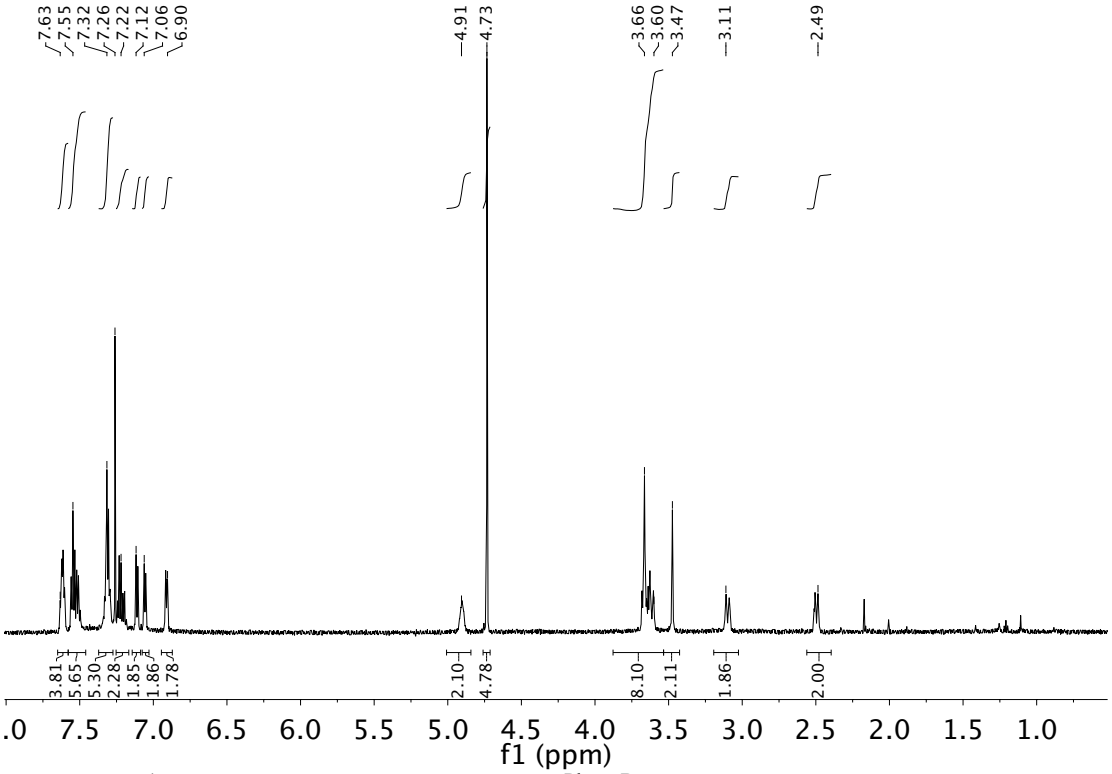

Figure S1: ^{1}H NMR spectrum of [Ru(Cp)($P^{Ph}_2N^{Bn}_2$)(benzylamine)]PF_6 (**3**) in $CDCl_3$.

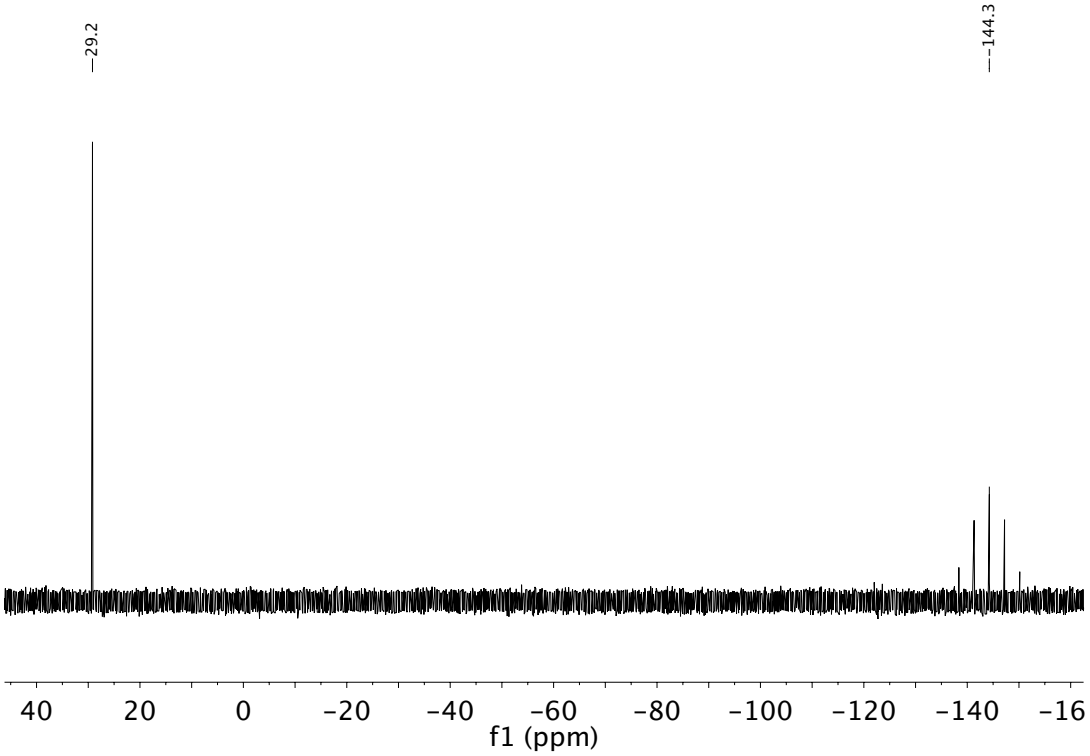

Figure S2: $^{31}P\{^{1}H\}$ NMR spectrum of [Ru(Cp)($P^{Ph}_2N^{Bn}_2$)(benzylamine)]PF_6 (**3**) in $CDCl_3$.

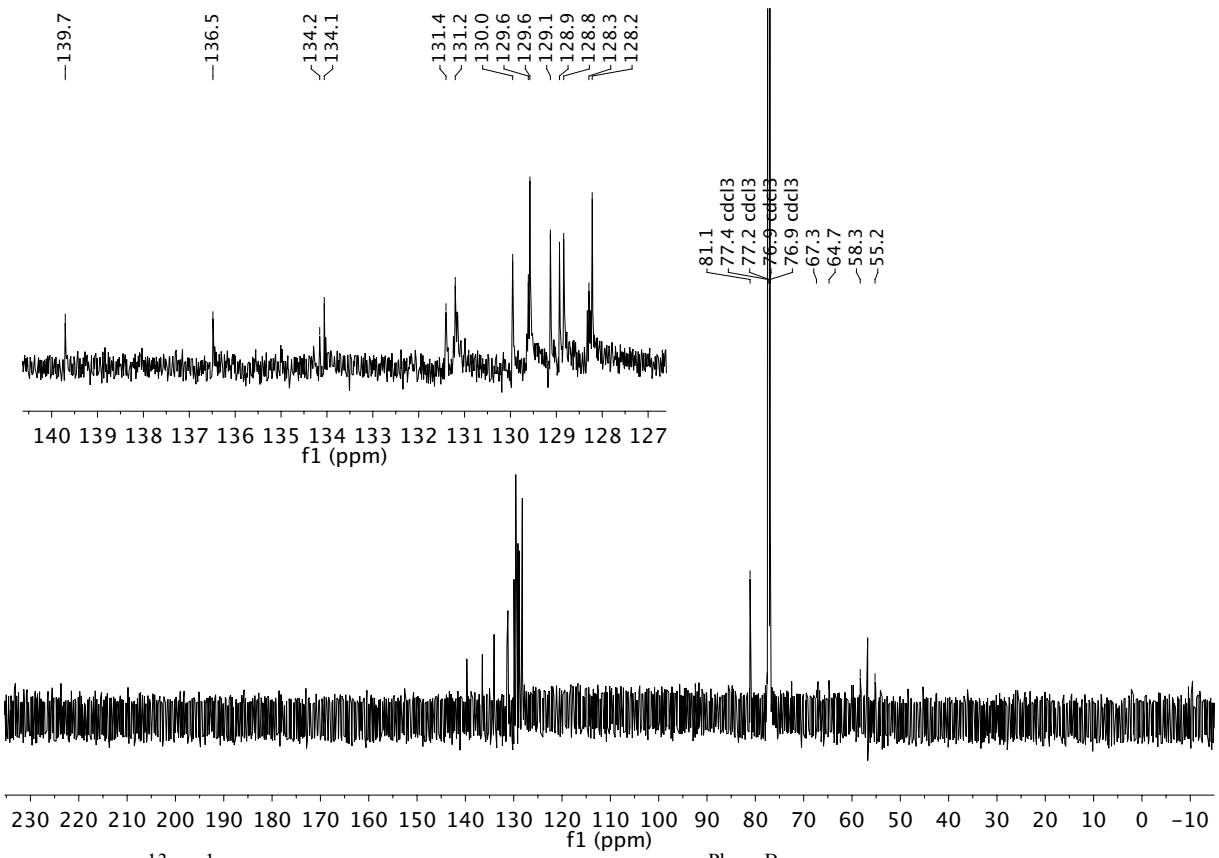

Figure S3: $^{13}C\{^{1}H\}$ (top) NMR spectrum of [Ru(Cp)($P^{Ph}{}_2N^{Bn}{}_2$)(benzylamine)]PF_6 (**3**) in $CDCl_3$. The inset displays a zoom-in of the aromatic carbon region.

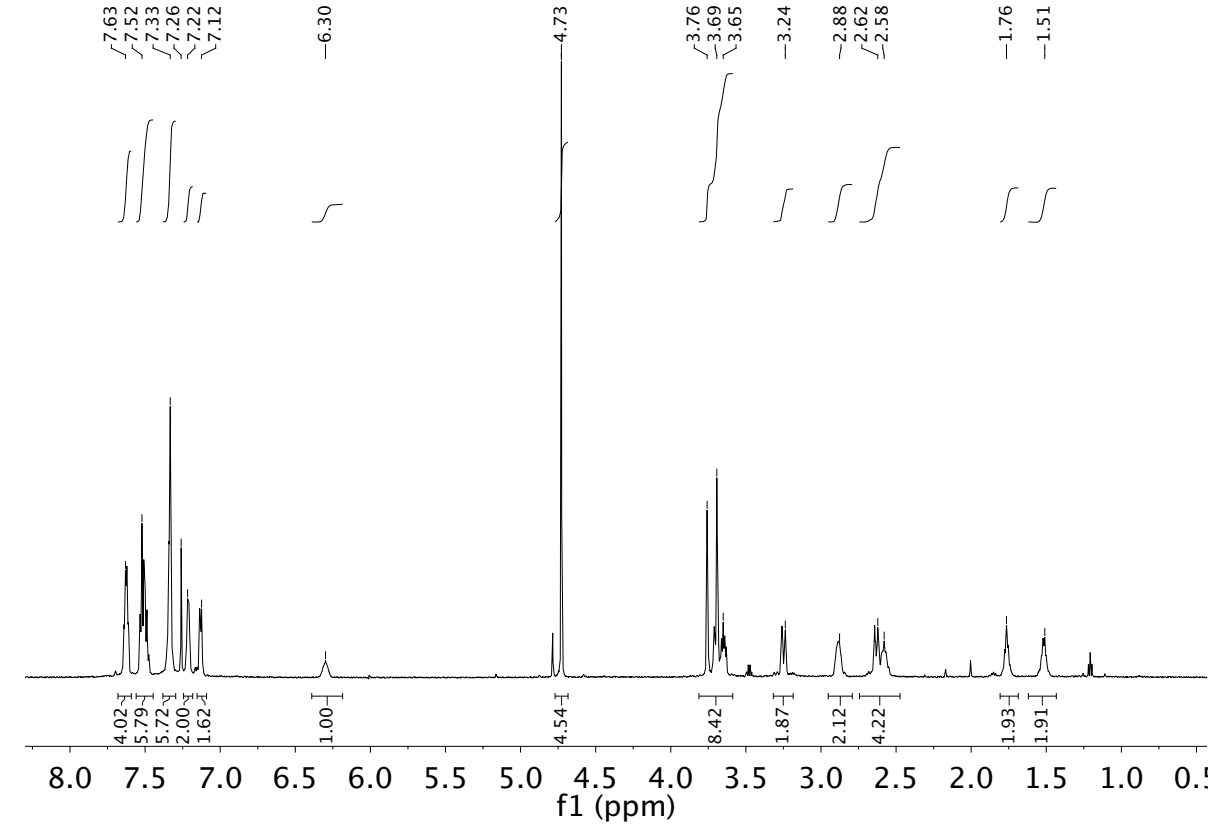

Figure S4: ^{1}H NMR spectrum of [Ru(Cp)($P^{Ph}{}_2N^{Bn}{}_2$)(pyrrolidine)]PF_6 (**4**) in $CDCl_3$.

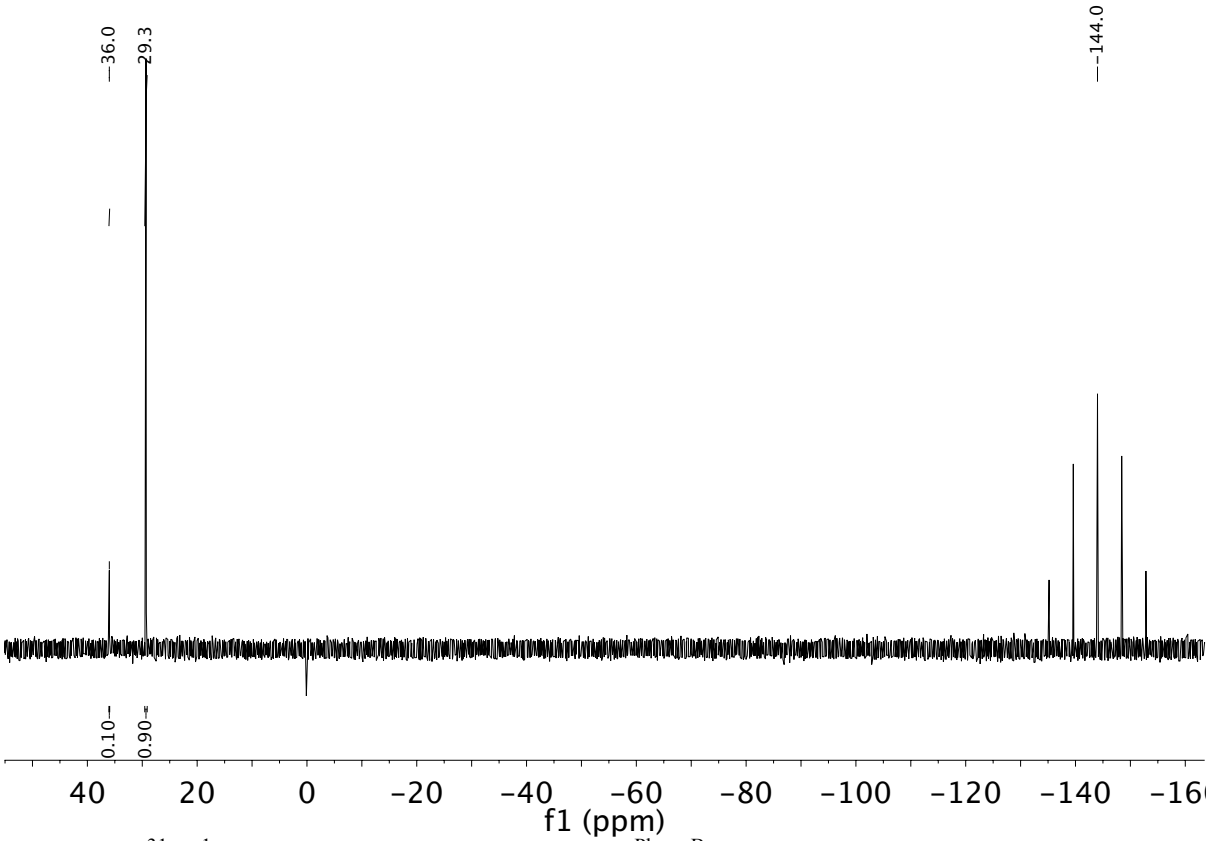

Figure S5: $^{31}P\{^{1}H\}$ NMR spectrum of [Ru(Cp)($P^{Ph}_2N^{Bn}_2$)(pyrrolidine)]PF_6 (**4**) in $CDCl_3$. Decomposition (36.0 ppm) is formed after analytically pure sample is dissolved in solution.

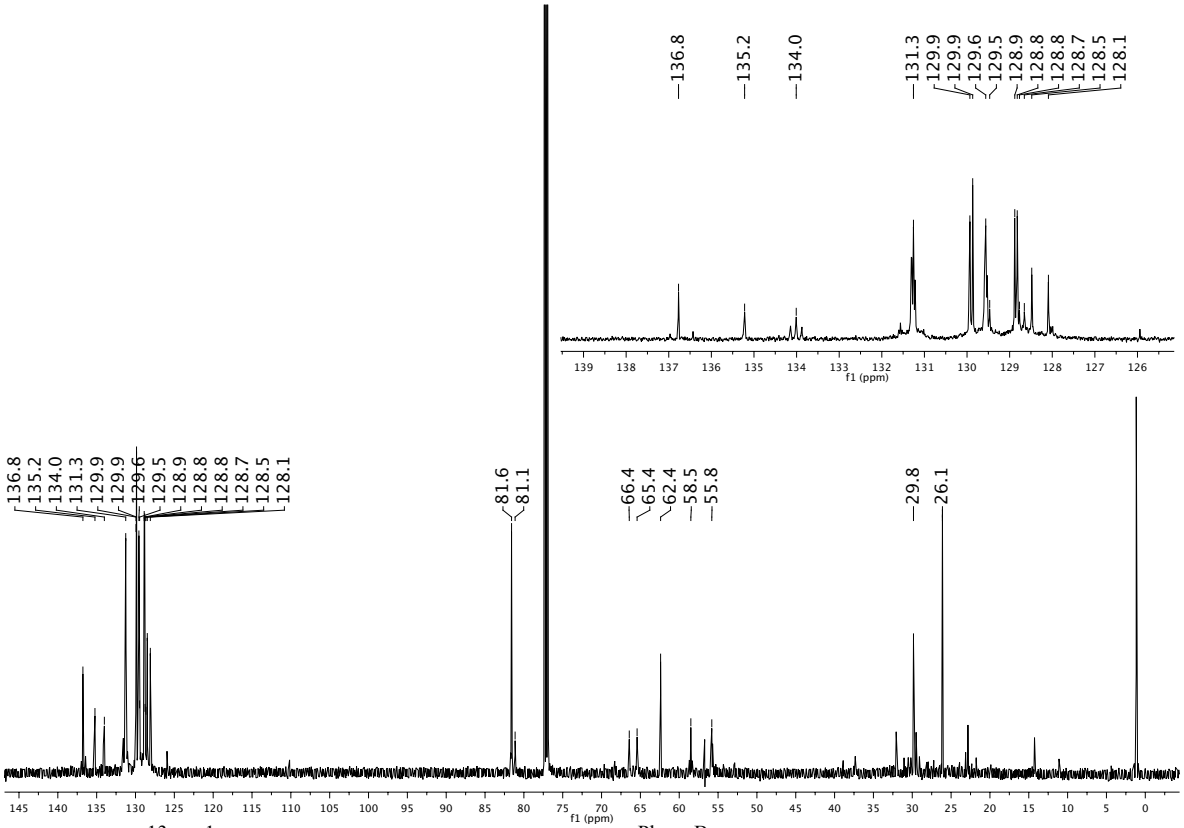

Figure S6: $^{13}C\{^{1}H\}$ NMR spectrum of [Ru(Cp)($P^{Ph}_2N^{Bn}_2$)(pyrrolidine)]PF_6 (**4**) in $CDCl_3$. The inset is a zoom-in of the aromatic carbon region.

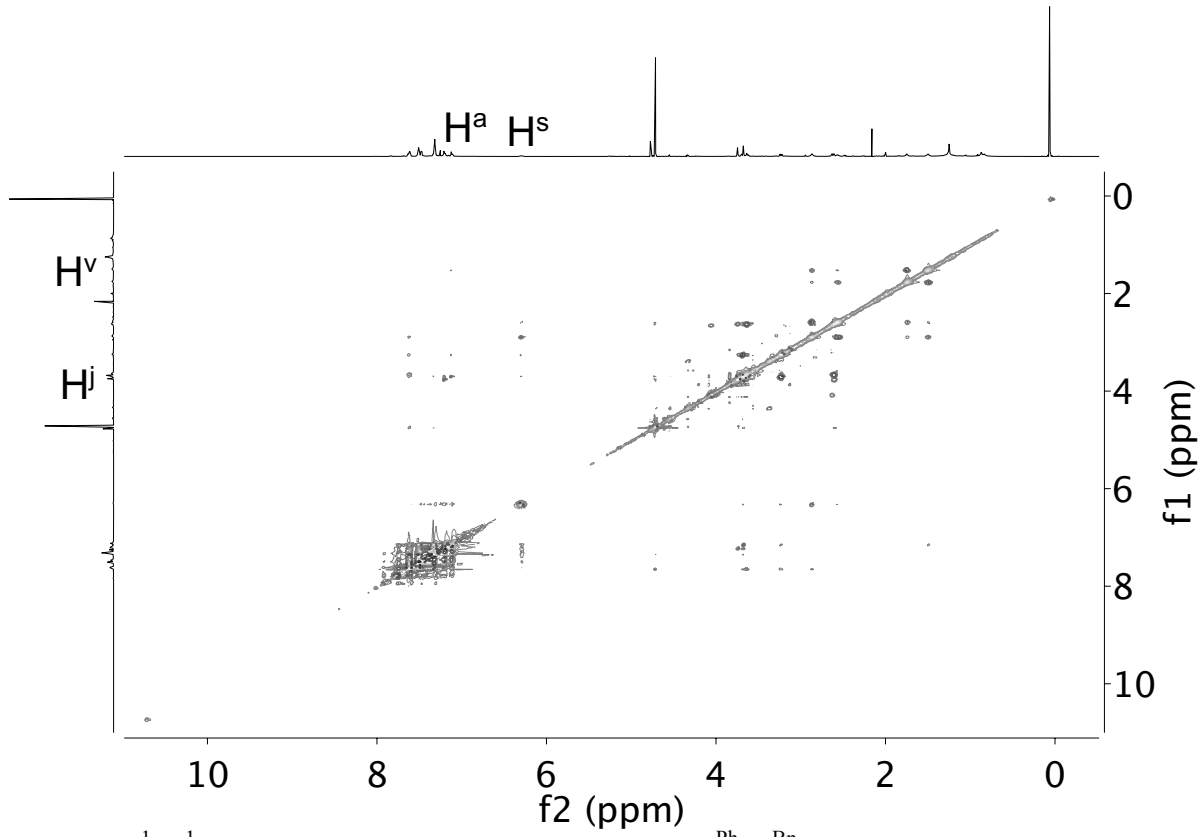

Figure S7: ^{1}H-^{1}H ROESY NMR spectrum of [Ru(Cp)($P^{Ph}_2N^{Bn}_2$)(pyrrolidine)]PF_6 (**4**) in $CDCl_3$.

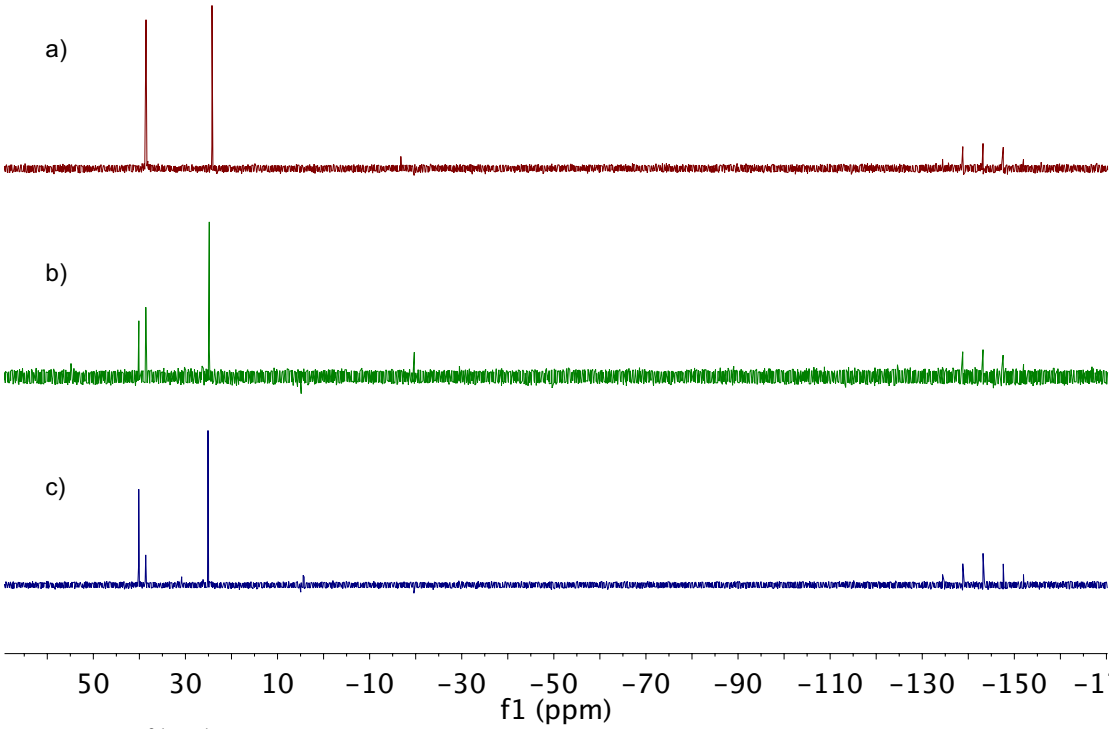

Figure S8: ^{31}P{^{1}H} NMR stacked spectra (proteo-THF) of a) [Ru(Cp)(dppp)(NCMe)]PF_6 (**2**) with O=PPh_3; and after addition of 5 eq. pyrrolidine at b) 4 h, **2** (38.6 ppm, 35%), **5** (40.1 ppm, 27%), missing (38%); and c) 21 h: **2** (38.6 ppm, 15%), **5** (40.1 ppm, 50%), missing (35%). Species at 40.1 ppm assigned to [Ru(Cp)(dppp)(pyrrolidine)]PF_6, **5,** is not stable to isolation.

II – Catalysis Graphs

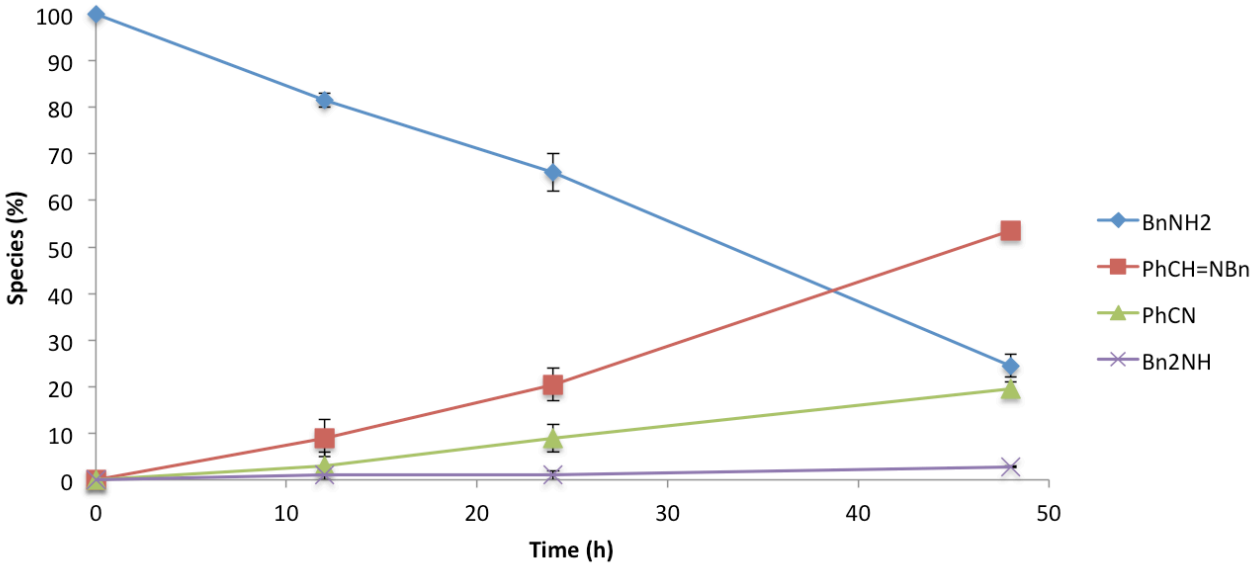

Figure S9**.** – Acceptorless dehydrogenation of benzylamine (250 mM) with 3 mol% **1** at 110 ˚C in anisole monitored over 48 h. Amounts were determined by GC-FID by area count of calibrated signals relative to an internal standard. Reactions were conducted in duplicate. Data points represent the average of the two runs and the error bars give the span of the conversion values of each data set.

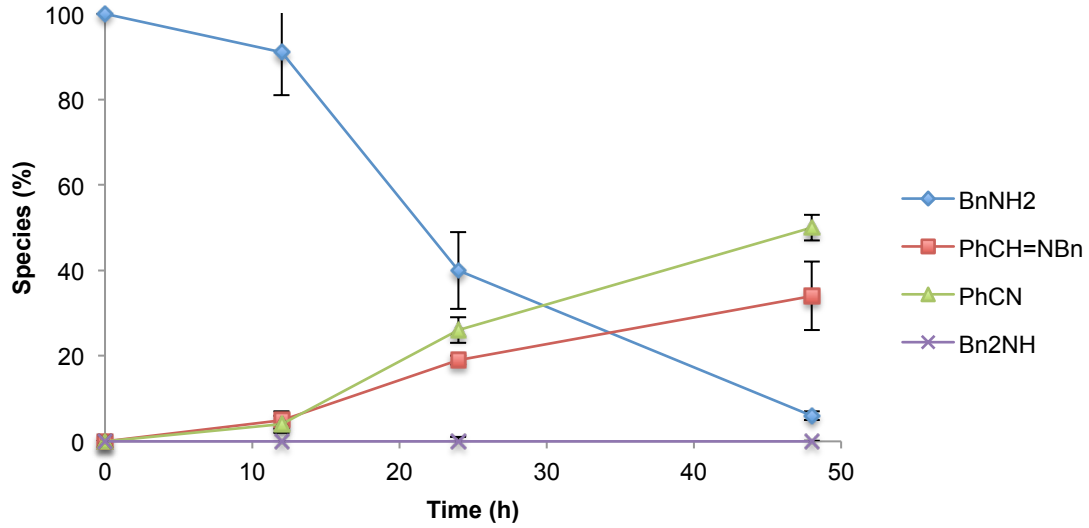

Figure S10**.** – Acceptorless dehydrogenation of benzylamine (250 mM) with 3 mol% **1** with 100 µL of mercury at 110 ˚C in anisole monitored over 48 h. Amounts were determined by GC-FID by area count of calibrated signals relative to an internal standard. Reactions were conducted in duplicate. Data points represent the average of the two runs and the error bars give the span of the conversion values of each data set.

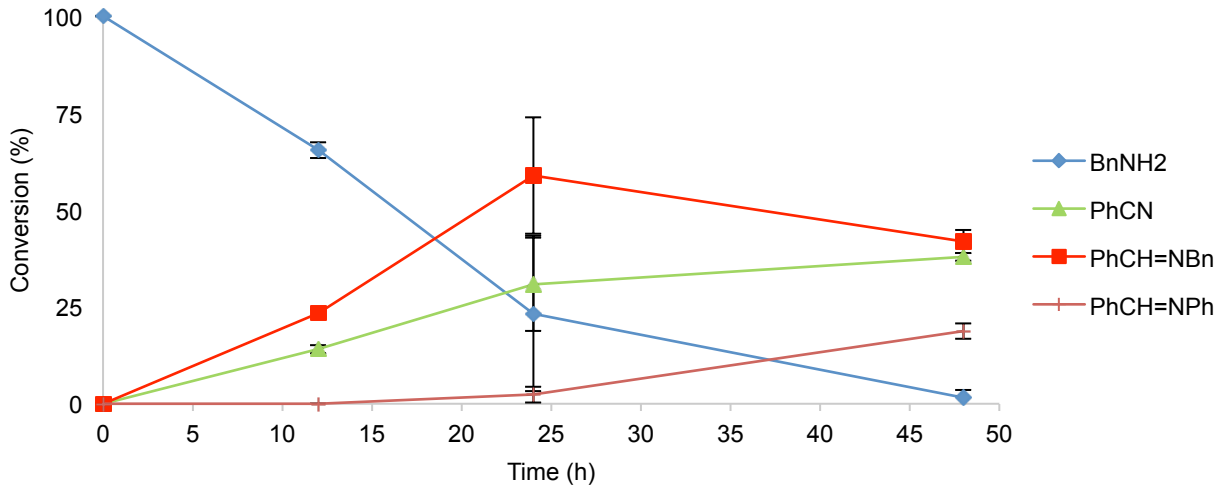

Figure S11**.** – Acceptorless dehydrogenation of benzylamine (250 mM) and aniline (250mM) with 3 mol% **1** at 110 ˚C in anisole monitored over 48 h. Amounts were determined by GC-FID by area count of calibrated signals relative to an internal standard. Reactions were conducted in duplicate. Data points represent the average of the two runs and the error bars give the span of the conversion values of each data set.

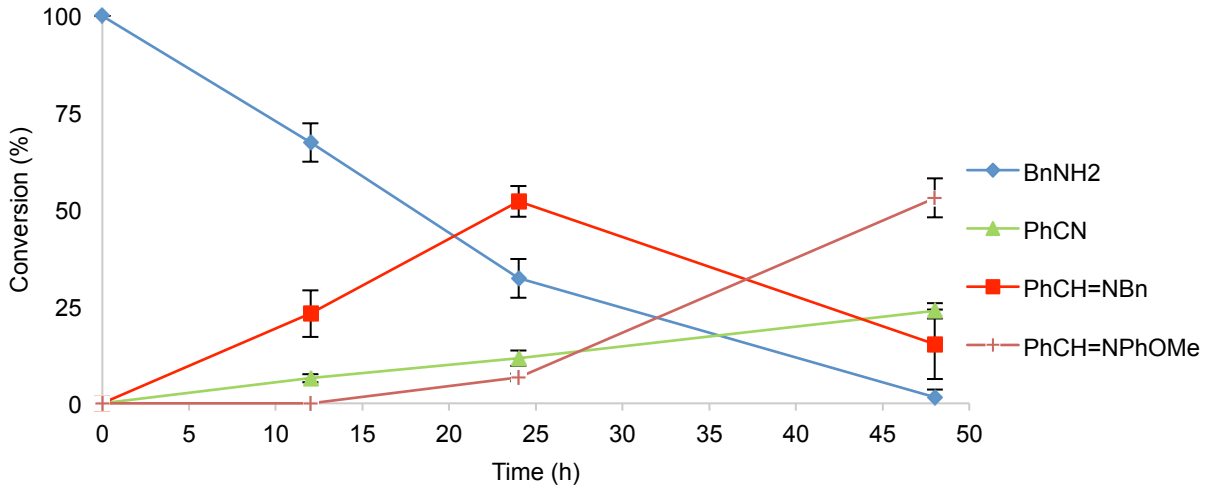

Figure S12**.** – Acceptorless dehydrogenation of benzylamine (250 mM) and p-anisidine (250mM) with 3 mol% **1** at 110 ˚C in anisole monitored over 48 h. Amounts were determined by GC-FID by area count of calibrated signals relative to an internal standard. Reactions were conducted in duplicate. Data points represent the average of the two runs and the error bars give the span of the conversion values of each data set.

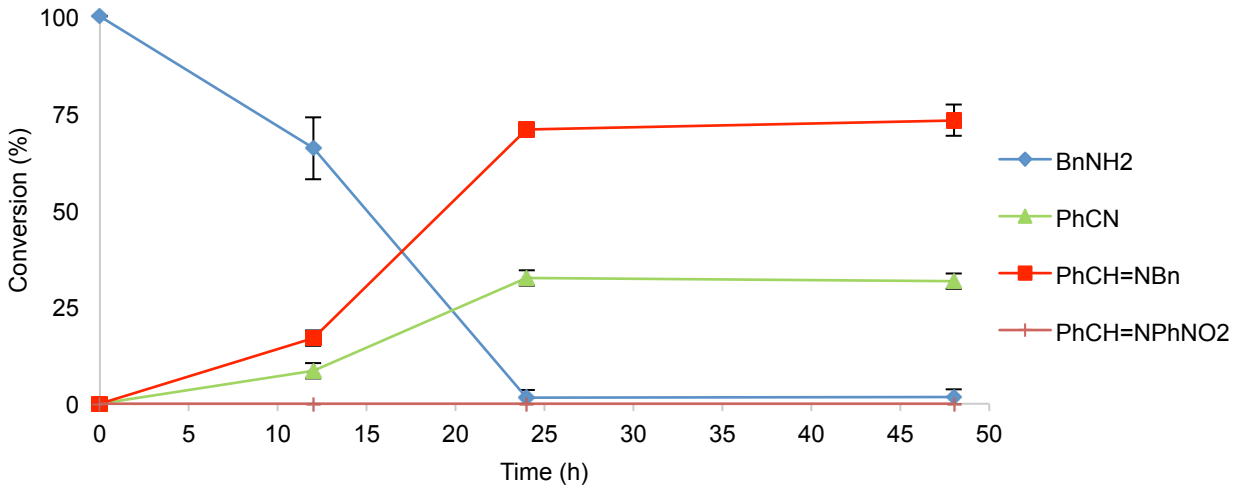

Figure S13**.** – Acceptorless dehydrogenation of benzylamine (250 mM) and p-nitroaniline (250mM) with 3 mol% **1** at 110 ˚C in anisole monitored over 48 h. Amounts were determined by GC-FID by area count of calibrated signals relative to an internal standard. Reactions were conducted in duplicate. Data points represent the average of the two runs and the error bars give the span of the conversion values of each data set.

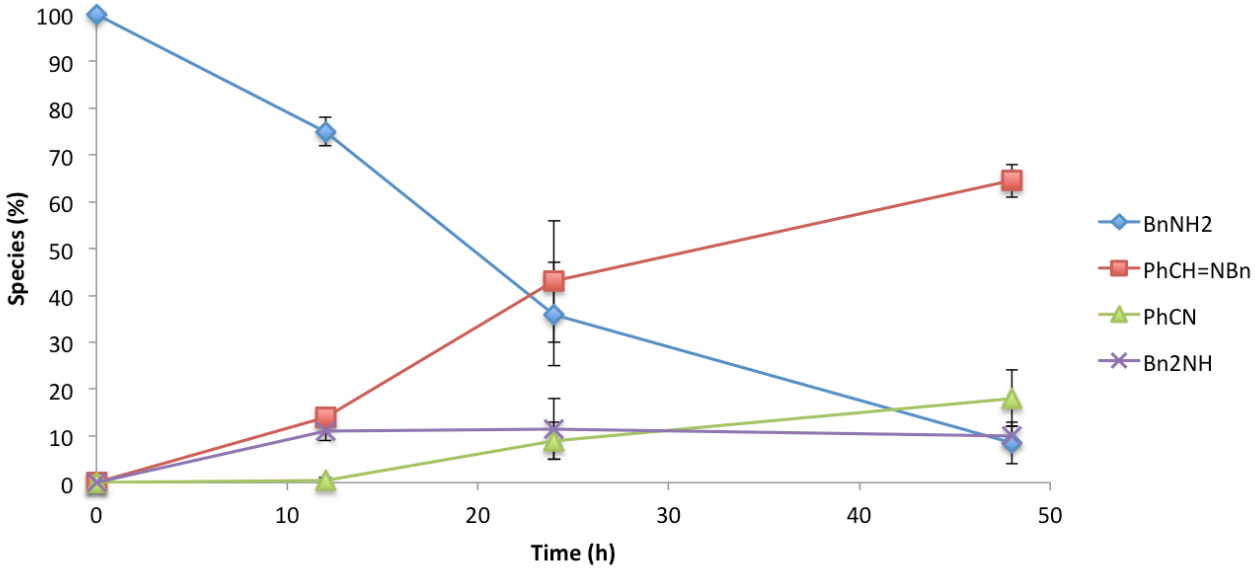

Figure S14**.** – Acceptorless dehydrogenation of benzylamine (250 mM) with 3 mol% **2** at 110 ˚C in anisole monitored over 48 h. Amounts were determined by GC-FID by area count of calibrated signals relative to an internal standard. Reactions were conducted in duplicate. Data points represent the average of the two runs and the error bars give the span of the conversion values of each data set.

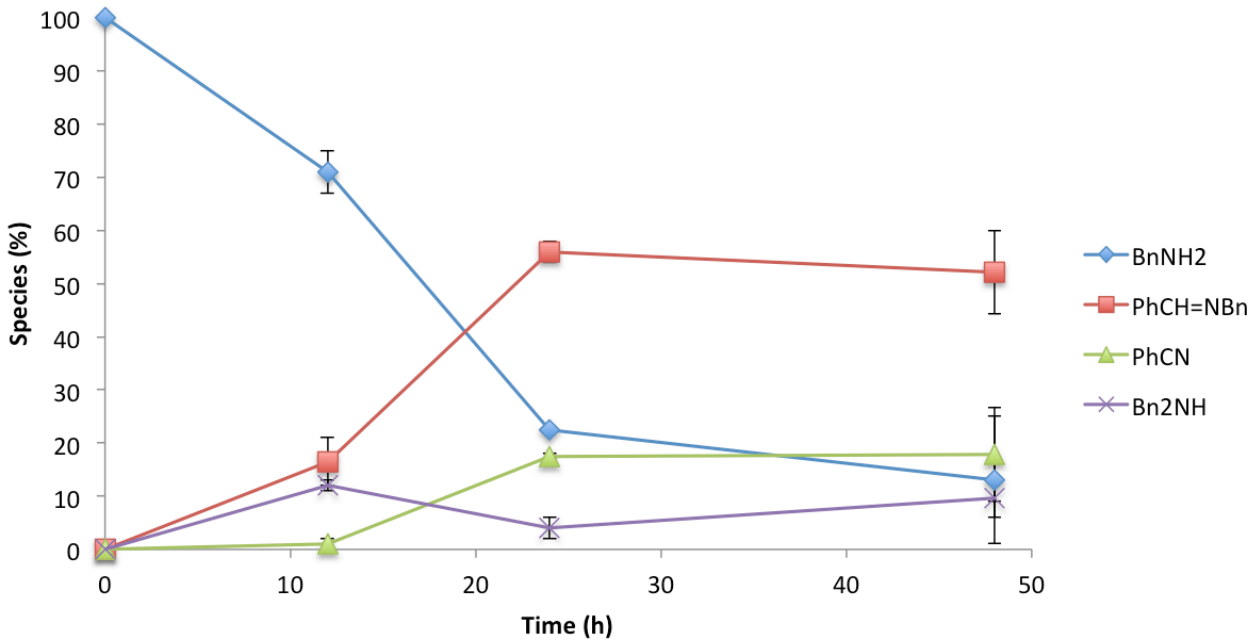

Figure S15**.** – Acceptorless dehydrogenation of benzylamine (250 mM) with 3 mol% **2** and 5 equiv. NEt_3 at 110 ˚C in anisole monitored over 48 h. Amounts were determined by GC-FID by area count of calibrated signals relative to an internal standard. Reactions were conducted in duplicate. Data points represent the average of the two runs and the error bars give the span of the conversion values of each data set.

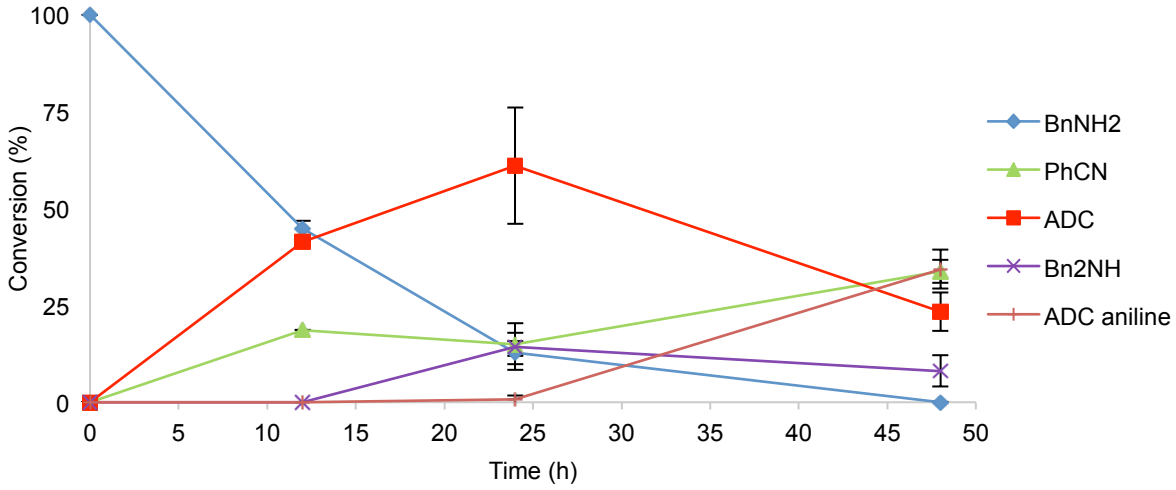

Figure S16**.** – Acceptorless dehydrogenation of benzylamine (250 mM) and aniline (250 mM) with 3 mol% **2** at 110 ˚C in anisole monitored over 48 h. Amounts were determined by GC-FID by area count of calibrated signals relative to an internal standard. Reactions were conducted in duplicate. Data points represent the average of the two runs and the error bars give the span of the conversion values of each data set.

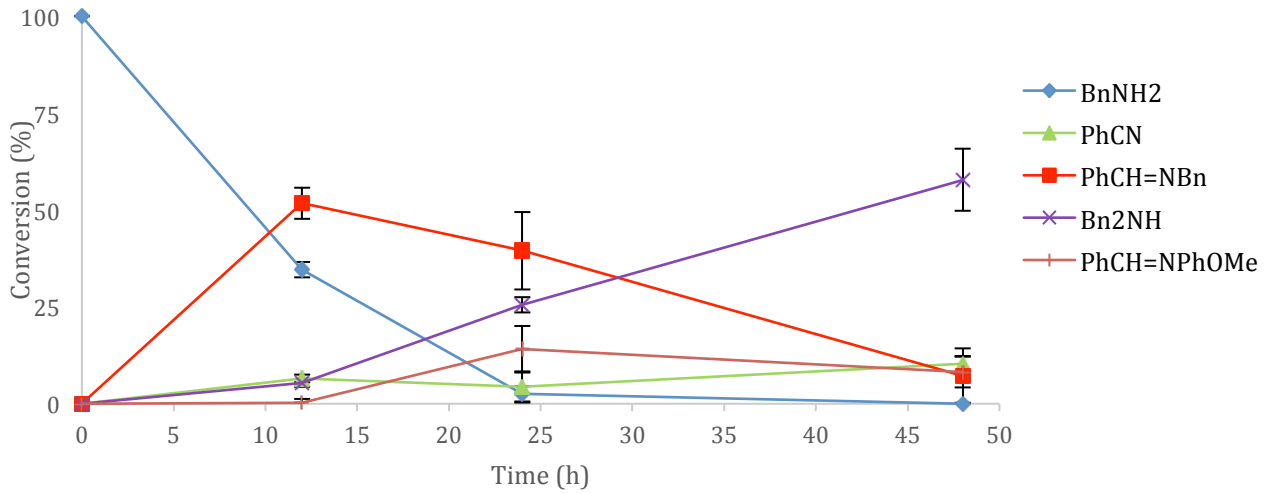

Figure S17**.** – Acceptorless dehydrogenation of benzylamine (250 mM) and p-anisidine (250 mM) with 3 mol% **2** at 110 ˚C in anisole monitored over 48 h. Amounts were determined by GC-FID by area count of calibrated signals relative to an internal standard. Reactions were conducted in duplicate. Data points represent the average of the two runs and the error bars give the span of the conversion values of each data set.

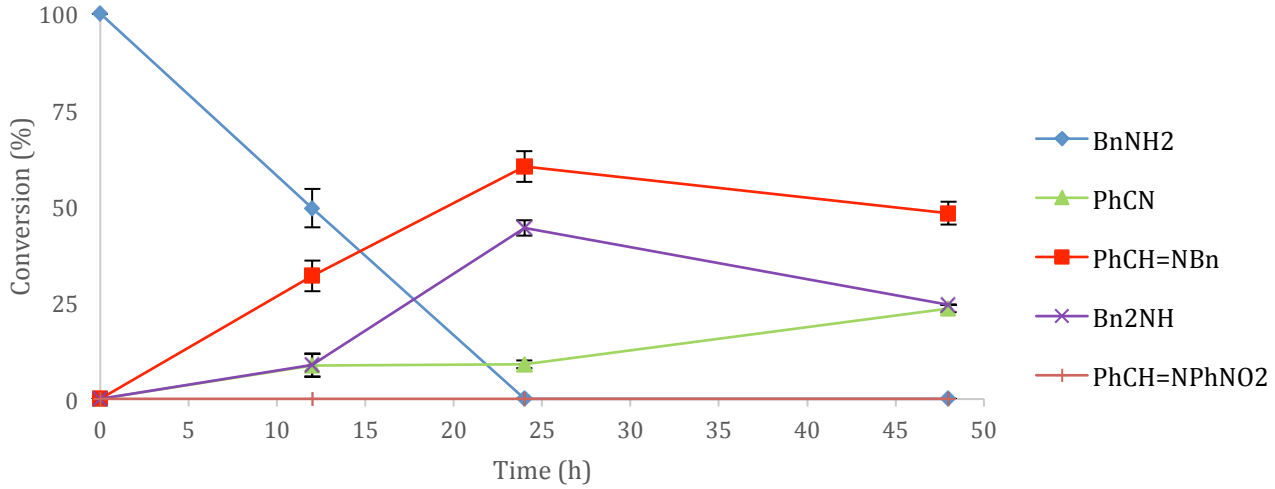

Figure S18**.** – Acceptorless dehydrogenation of benzylamine (250 mM) and p-nitroaniline (250 mM) with 3 mol% **2** at 110 ˚C in anisole monitored over 48 h. Amounts were determined by GC-FID by area count of calibrated signals relative to an internal standard. Reactions were conducted in duplicate. Data points represent the average of the two runs and the error bars give the span of the conversion values of each data set.

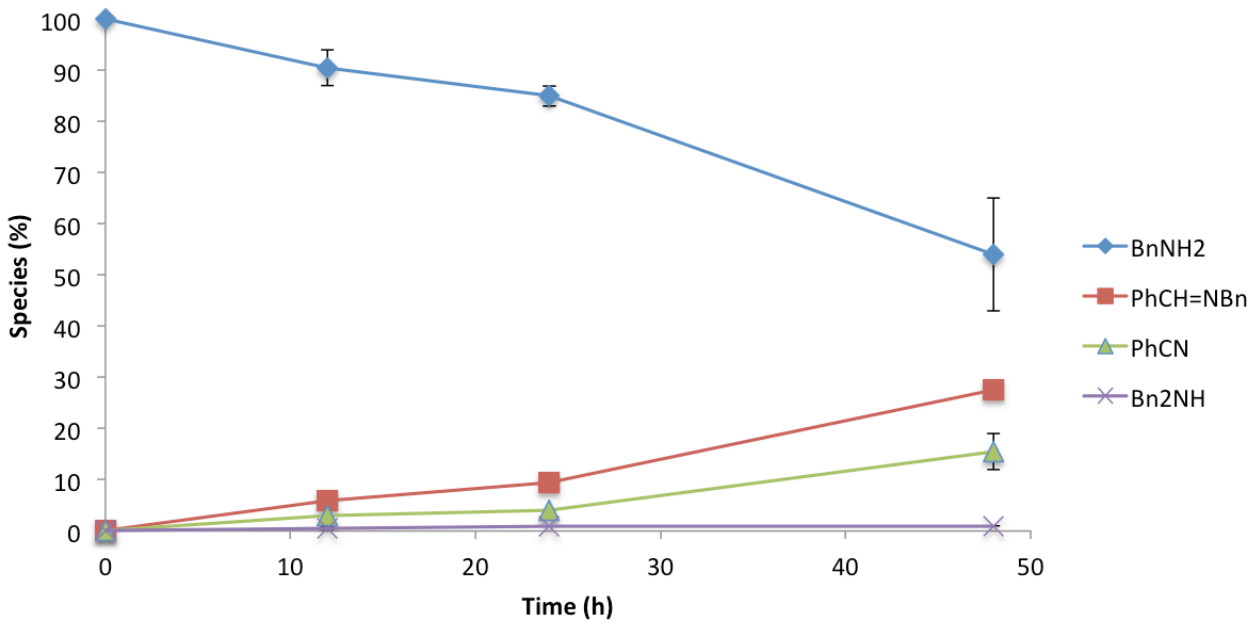

Figure S19**.** – Acceptorless dehydrogenation of benzylamine (250 mM) with 3 mol% **3** at 110 ˚C in anisole monitored over 48 h. Amounts were determined by GC-FID by area count of calibrated signals relative to an internal standard. Reactions were conducted in duplicate. Data points represent the average of the two runs and the error bars give the span of the conversion values of each data set.

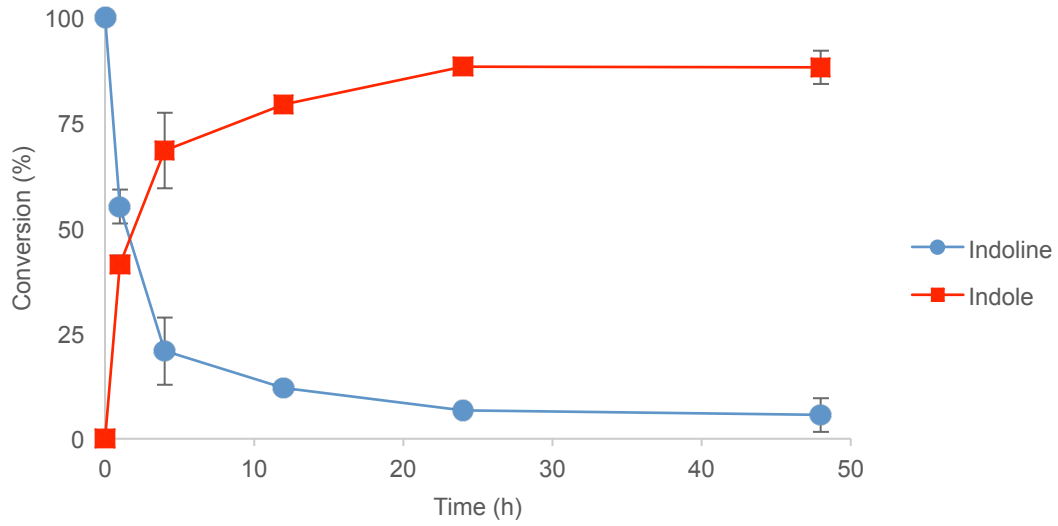

Figure S20**.** – Acceptorless dehydrogenation of indoline (250 mM) with 3 mol% **1** at 110 ˚C in anisole monitored over 48 h. Amounts were determined by GC-FID by area count of calibrated signals relative to an internal standard. Reactions were conducted in duplicate. Data points represent the average of the two runs and the error bars give the span of the conversion values of each data set.

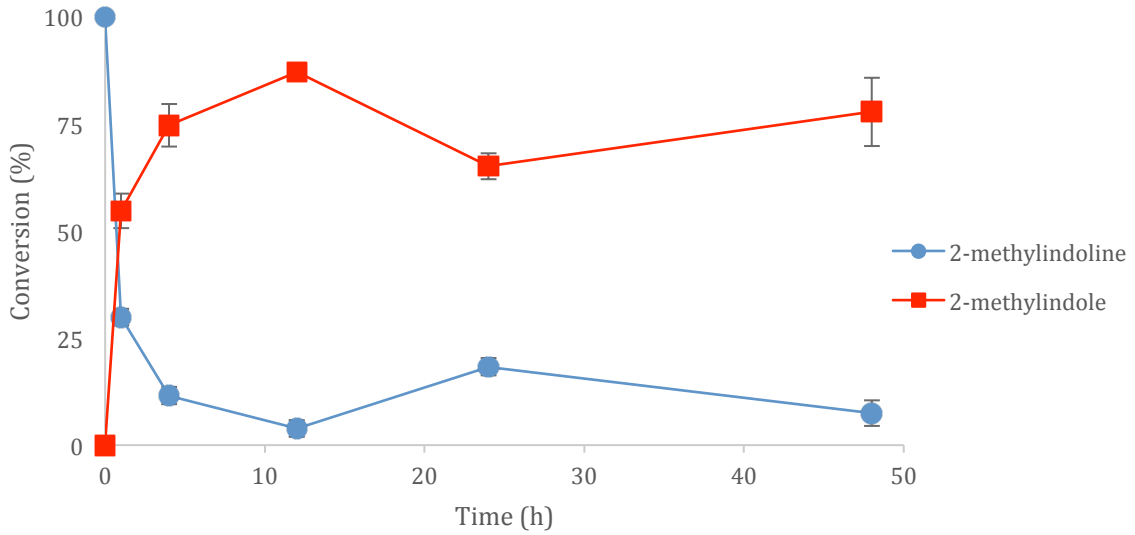

Figure S21**.** – Acceptorless dehydrogenation of 2-methylindoline (250 mM) with 3 mol% **1** at 110 ˚C in anisole monitored over 48 h. Amounts were determined by GC-FID by area count of calibrated signals relative to an internal standard. Reactions were conducted in duplicate. Data points represent the average of the two runs and the error bars give the span of the conversion values of each data set.

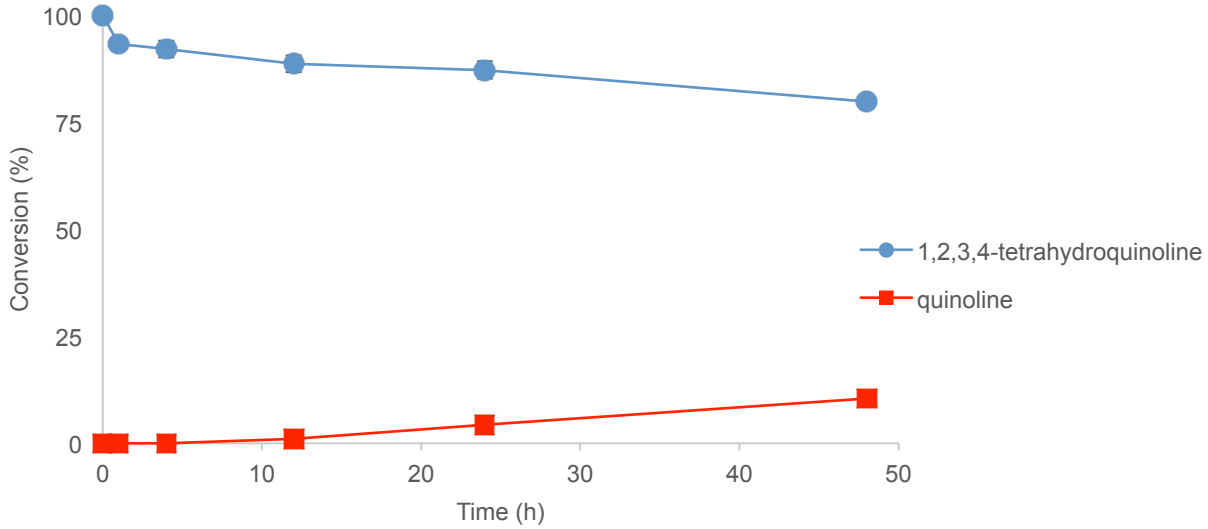

Figure S22**.** – Acceptorless dehydrogenation of 1,2,3,4-tetrahydroquinoline (250 mM) with 3 mol% **1** at 110 ˚C in anisole monitored over 48 h. Amounts were determined by GC-FID by area count of calibrated signals relative to an internal standard. Reactions were conducted in duplicate. Data points represent the average of the two runs and the error bars give the span of the conversion values of each data set.

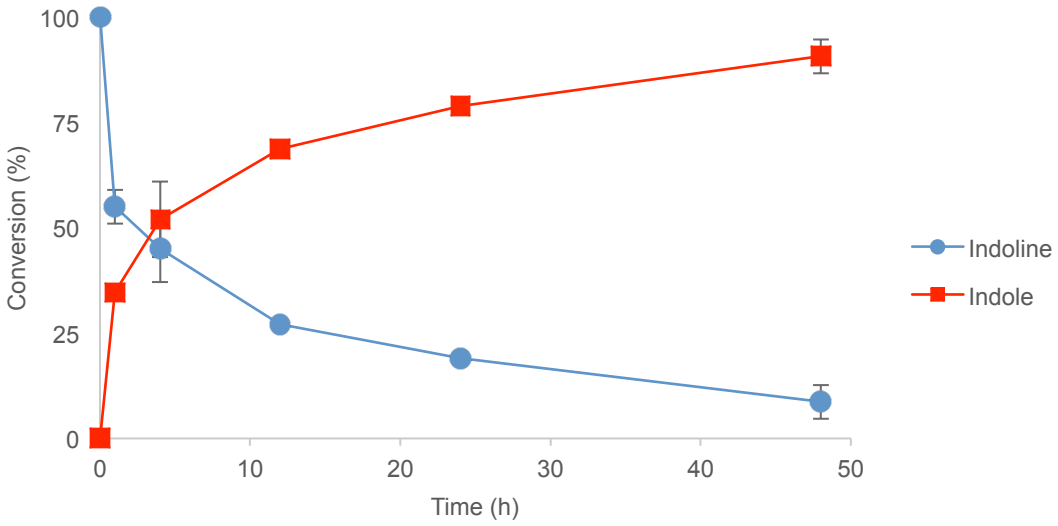

Figure S23**.** – Acceptorless dehydrogenation of indoline (250 mM) with 3 mol% **2** at 110 ˚C in anisole monitored over 48 h. Amounts were determined by GC-FID by area count of calibrated signals relative to an internal standard. Reactions were conducted in duplicate. Data points represent the average of the two runs and the error bars give the span of the conversion values of each data set.

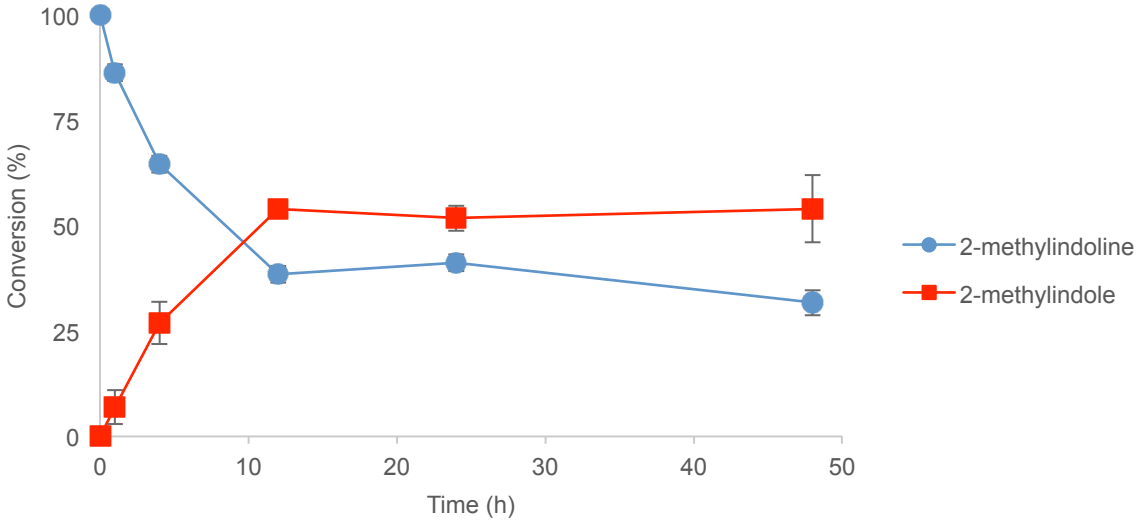

Figure S24**.** – Acceptorless dehydrogenation of 2-methylindoline (250 mM) with 3 mol% **2** at 110 ˚C in anisole monitored over 48 h. Amounts were determined by GC-FID by area count of calibrated signals relative to an internal standard. Reactions were conducted in duplicate. Data points represent the average of the two runs and the error bars give the span of the conversion values of each data set.

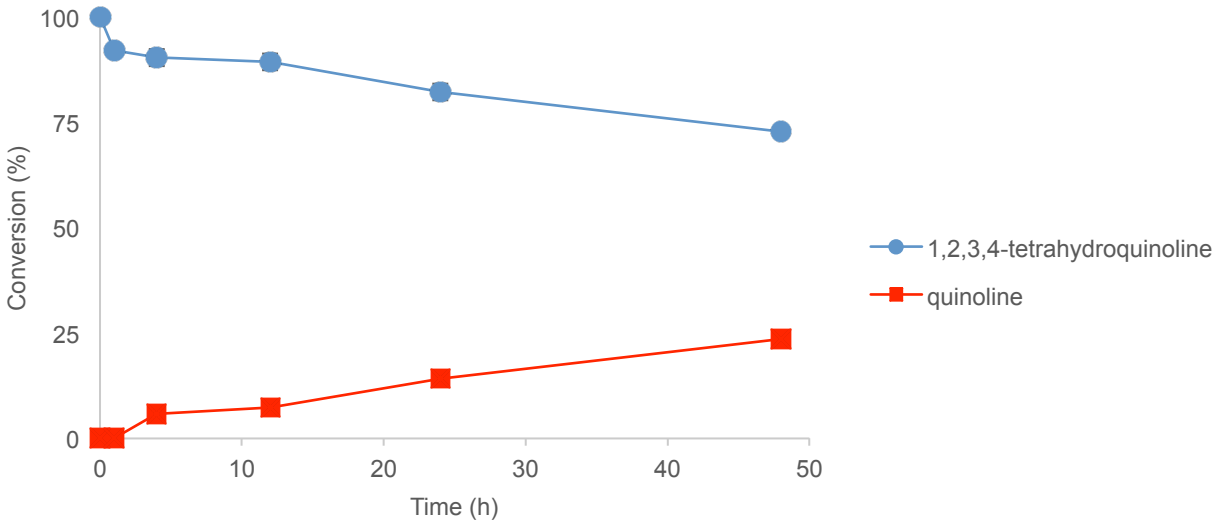

Figure S25**.** – Acceptorless dehydrogenation of 1,2,3,4-tetrahydroquinoline (250 mM) with 3 mol% **2** at 110 ˚C in anisole monitored over 48 h. Amounts were determined by GC-FID by area count of calibrated signals relative to an internal standard. Reactions were conducted in duplicate. Data points represent the average of the two runs and the error bars give the span of the conversion values of each data set.

III – Crystallographic Details
Experimental for $C_{39}H_{46}F_6N_3P_3Ru$ (**4**), CCDC 1545183

Data Collection and Processing. The sample was mounted on a Mitegen polyimide micromount with a small amount of Paratone N oil. All X-ray measurements were made on a Bruker Kappa Axis Apex2 diffractometer at a temperature of 110 K. The unit cell dimensions were determined from a symmetry constrained fit of 9960 reflections with 5.16° < 2q < 51.32°. The data collection strategy was a number of w and j scans which collected data up to 51.722° (2q). The frame integration was performed using SAINT.[1] The resulting raw data was scaled and absorption corrected using a multi-scan averaging of symmetry equivalent data using SADABS.[2]

Structure Solution and Refinement. The structure was solved by using a dual space methodology using the SHELXT program.[3] All non-hydrogen atoms were obtained from the initial solution. The hydrogen atoms were introduced at idealized positions and were allowed to ride on the parent atom. The structural model was fit to the data using full matrix least-squares based on F^2. The calculated structure factors included corrections for anomalous dispersion from the usual tabulation. The structure was refined using the SHELXL-2014 program from the SHELX suite of crystallographic software.[4] Graphic plots were produced using the NRCVAX program suite.[5]

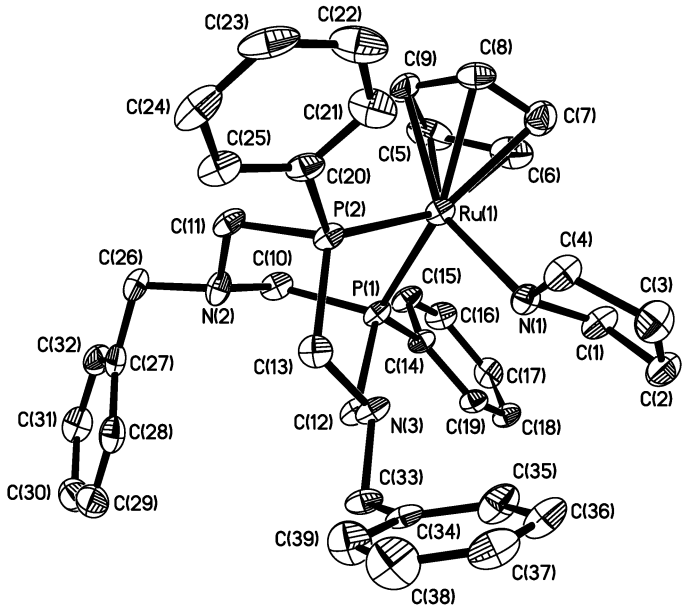

Figure S26. ORTEP drawing of **4** showing naming and numbering scheme. Ellipsoids are at the 50% probability level and hydrogen atoms were omitted for clarity. PF_6 counter-ion was omitted for clarity.

Table S1. Summary of Crystal Data for **4**

Formula	$C_{39}H_{46}F_6N_3P_3Ru$
CCDC	1545183
Formula Weight (*g/mol*)	864.77
Crystal Dimensions (*mm*)	0.165 × 0.069 × 0.037
Crystal Color and Habit	yellow plate
Crystal System	monoclinic
Space Group	P 2_1/n
Temperature, K	110
a, Å	10.564(3)
b, Å	23.741(9)
c, Å	15.120(6)
α,°	90
β,°	90.179(13)
γ,°	90
V, Å^3	3792(2)
Number of reflections to determine final unit cell	9960
Min and Max 2θ for cell determination, °	5.16, 51.32
Z	4
F(000)	1776
ρ (*g/cm*)	1.515
λ, Å, (MoKα)	0.71073
μ, (cm^{-1})	0.603
Diffractometer Type	Bruker Kappa Axis Apex2
Scan Type(s)	φ and ω scans
Max 2θ for data collection, °	51.722
Measured fraction of data	0.998
Number of reflections measured	63314
Unique reflections measured	7239
R_{merge}	0.1119
Number of reflections included in refinement	7239
Cut off Threshold Expression	$I > 2\sigma(I)$
Structure refined using	full matrix least-squares using F^2
Weighting Scheme	$w=1/[\sigma^2(Fo^2)+(0.0841P)^2+5.2475P]$ where $P=(Fo^2+2Fc^2)/3$

Number of parameters in least-squares	469
R_1	0.0653
wR_2	0.1478
R_1 (all data)	0.1124
wR_2 (all data)	0.1718
GOF	1.056
Maximum shift/error	0.001
Min & Max peak heights on final ΔF Map (e^-/Å)	-1.363, 2.418

Where:
$R_1 = \Sigma(|F_o| - |F_c|) / \Sigma F_o$
$wR_2 = [\Sigma(w(F_o^2 - F_c^2)^2) / \Sigma(w F_o^4)]^{½}$
GOF = $[\Sigma(w(F_o^2 - F_c^2)^2) / (\text{No. of reflns. - No. of params.})]^{½}$

Table S2. Bond Lengths for **4**

Ru1-N1	2.163(4)	C15-C16	1.366(8)
Ru1-C5	2.190(6)	C15-H15	0.9500
Ru1-C9	2.201(6)	C16-C17	1.388(8)
Ru1-C6	2.238(6)	C16-H16	0.9500
Ru1-C8	2.252(6)	C17-C18	1.379(8)
Ru1-C7	2.253(7)	C17-H17	0.9500
Ru1-P1	2.2564(17)	C18-C19	1.385(8)
Ru1-P2	2.2646(17)	C18-H18	0.9500
P1-C14	1.809(6)	C19-H19	0.9500
P1-C10	1.839(6)	C20-C21	1.379(9)
P1-C12	1.861(5)	C20-C25	1.382(8)
P2-C20	1.841(6)	C21-C22	1.387(9)
P2-C13	1.854(6)	C21-H21	0.9500
P2-C11	1.855(6)	C22-C23	1.377(10)
N1-C1	1.475(8)	C22-H22	0.9500
N1-C4	1.493(7)	C23-C24	1.387(10)
N1-H1	1.0000	C23-H23	0.9500
N2-C11	1.453(7)	C24-C25	1.390(8)
N2-C10	1.455(7)	C24-H24	0.9500
N2-C26	1.482(7)	C25-H25	0.9500
N3-C13	1.461(7)	C26-C27	1.491(8)
N3-C12	1.483(7)	C26-H26A	0.9900

N3-C33	1.484(7)	C26-H26B	0.9900
C1-C2	1.523(8)	C27-C32	1.392(8)
C1-H1A	0.9900	C27-C28	1.403(8)
C1-H1B	0.9900	C28-C29	1.366(9)
C2-C3	1.536(9)	C28-H28	0.9500
C2-H2A	0.9900	C29-C30	1.389(9)
C2-H2B	0.9900	C29-H29	0.9500
C3-C4	1.534(8)	C30-C31	1.389(9)
C3-H3A	0.9900	C30-H30	0.9500
C3-H3B	0.9900	C31-C32	1.384(9)
C4-H4A	0.9900	C31-H31	0.9500
C4-H4B	0.9900	C32-H32	0.9500
C5-C9	1.408(9)	C33-C34	1.509(7)
C5-C6	1.422(10)	C33-H33A	0.9900
C5-H5	0.9500	C33-H33B	0.9900
C6-C7	1.388(9)	C34-C35	1.380(9)
C6-H6	0.9500	C34-C39	1.385(8)
C7-C8	1.388(9)	C35-C36	1.405(8)
C7-H7	0.9500	C35-H35	0.9500
C8-C9	1.439(9)	C36-C37	1.361(9)
C8-H8	0.9500	C36-H36	0.9500
C9-H9	0.9500	C37-C38	1.358(10)
C10-H10A	0.9900	C37-H37	0.9500
C10-H10B	0.9900	C38-C39	1.401(9)
C11-H11A	0.9900	C38-H38	0.9500
C11-H11B	0.9900	C39-H39	0.9500
C12-H12A	0.9900	P3-F4	1.581(4)
C12-H12B	0.9900	P3-F1	1.595(4)
C13-H13A	0.9900	P3-F2	1.596(4)
C13-H13B	0.9900	P3-F5	1.597(4)
C14-C19	1.391(7)	P3-F6	1.600(4)
C14-C15	1.418(7)	P3-F3	1.608(4)

Table S3. Bond Angles for **4**

N1-Ru1-C5	143.4(2)	N2-C11-H11B	109.2
N1-Ru1-C9	151.0(2)	P2-C11-H11B	109.2
C5-Ru1-C9	37.4(3)	H11A-C11-H11B	107.9
N1-Ru1-C6	106.7(2)	N3-C12-P1	112.8(4)
C5-Ru1-C6	37.4(3)	N3-C12-H12A	109.0
C9-Ru1-C6	62.2(3)	P1-C12-H12A	109.0
N1-Ru1-C8	113.4(2)	N3-C12-H12B	109.0
C5-Ru1-C8	62.1(2)	P1-C12-H12B	109.0
C9-Ru1-C8	37.7(2)	H12A-C12-H12B	107.8
C6-Ru1-C8	60.9(2)	N3-C13-P2	113.6(4)
N1-Ru1-C7	93.4(2)	N3-C13-H13A	108.8
C5-Ru1-C7	61.3(2)	P2-C13-H13A	108.8
C9-Ru1-C7	61.4(2)	N3-C13-H13B	108.8
C6-Ru1-C7	36.0(2)	P2-C13-H13B	108.8
C8-Ru1-C7	35.9(2)	H13A-C13-H13B	107.7
N1-Ru1-P1	91.91(13)	C19-C14-C15	117.6(5)
C5-Ru1-P1	92.29(18)	C19-C14-P1	122.0(4)
C9-Ru1-P1	116.38(19)	C15-C14-P1	120.2(4)
C6-Ru1-P1	104.37(18)	C16-C15-C14	120.7(5)
C8-Ru1-P1	153.10(15)	C16-C15-H15	119.6
C7-Ru1-P1	139.37(18)	C14-C15-H15	119.6
N1-Ru1-P2	93.76(13)	C15-C16-C17	120.7(5)
C5-Ru1-P2	122.7(2)	C15-C16-H16	119.7
C9-Ru1-P2	97.43(18)	C17-C16-H16	119.7
C6-Ru1-P2	158.98(19)	C18-C17-C16	119.7(5)
C8-Ru1-P2	106.71(17)	C18-C17-H17	120.2
C7-Ru1-P2	140.25(18)	C16-C17-H17	120.2
P1-Ru1-P2	79.32(6)	C17-C18-C19	120.1(5)
C14-P1-C10	103.3(3)	C17-C18-H18	120.0
C14-P1-C12	105.5(3)	C19-C18-H18	120.0
C10-P1-C12	100.0(3)	C18-C19-C14	121.2(5)
C14-P1-Ru1	116.7(2)	C18-C19-H19	119.4
C10-P1-Ru1	112.2(2)	C14-C19-H19	119.4
C12-P1-Ru1	117.07(18)	C21-C20-C25	119.0(6)
C20-P2-C13	103.5(2)	C21-C20-P2	119.3(5)

C20-P2-C11	100.5(3)	C25-C20-P2	121.7(5)
C13-P2-C11	100.7(3)	C20-C21-C22	121.5(7)
C20-P2-Ru1	121.6(2)	C20-C21-H21	119.3
C13-P2-Ru1	116.37(19)	C22-C21-H21	119.3
C11-P2-Ru1	111.21(19)	C23-C22-C21	119.2(7)
C1-N1-C4	104.7(4)	C23-C22-H22	120.4
C1-N1-Ru1	116.7(3)	C21-C22-H22	120.4
C4-N1-Ru1	115.8(3)	C22-C23-C24	120.1(6)
C1-N1-H1	106.3	C22-C23-H23	120.0
C4-N1-H1	106.3	C24-C23-H23	120.0
Ru1-N1-H1	106.3	C23-C24-C25	120.1(6)
C11-N2-C10	114.2(5)	C23-C24-H24	120.0
C11-N2-C26	110.1(4)	C25-C24-H24	120.0
C10-N2-C26	110.0(4)	C20-C25-C24	120.2(6)
C13-N3-C12	114.1(4)	C20-C25-H25	119.9
C13-N3-C33	109.6(4)	C24-C25-H25	119.9
C12-N3-C33	108.6(4)	N2-C26-C27	112.0(5)
N1-C1-C2	105.6(5)	N2-C26-H26A	109.2
N1-C1-H1A	110.6	C27-C26-H26A	109.2
C2-C1-H1A	110.6	N2-C26-H26B	109.2
N1-C1-H1B	110.6	C27-C26-H26B	109.2
C2-C1-H1B	110.6	H26A-C26-H26B	107.9
H1A-C1-H1B	108.8	C32-C27-C28	117.7(6)
C1-C2-C3	103.2(5)	C32-C27-C26	121.8(5)
C1-C2-H2A	111.1	C28-C27-C26	120.5(5)
C3-C2-H2A	111.1	C29-C28-C27	120.6(6)
C1-C2-H2B	111.1	C29-C28-H28	119.7
C3-C2-H2B	111.1	C27-C28-H28	119.7
H2A-C2-H2B	109.1	C28-C29-C30	121.3(6)
C4-C3-C2	105.7(5)	C28-C29-H29	119.4
C4-C3-H3A	110.6	C30-C29-H29	119.4
C2-C3-H3A	110.6	C31-C30-C29	119.1(7)
C4-C3-H3B	110.6	C31-C30-H30	120.5
C2-C3-H3B	110.6	C29-C30-H30	120.5
H3A-C3-H3B	108.7	C32-C31-C30	119.6(6)
N1-C4-C3	107.0(5)	C32-C31-H31	120.2

N1-C4-H4A	110.3	C30-C31-H31	120.2
C3-C4-H4A	110.3	C31-C32-C27	121.8(6)
N1-C4-H4B	110.3	C31-C32-H32	119.1
C3-C4-H4B	110.3	C27-C32-H32	119.1
H4A-C4-H4B	108.6	N3-C33-C34	112.5(5)
C9-C5-C6	108.1(6)	N3-C33-H33A	109.1
C9-C5-Ru1	71.7(3)	C34-C33-H33A	109.1
C6-C5-Ru1	73.1(3)	N3-C33-H33B	109.1
C9-C5-H5	125.9	C34-C33-H33B	109.1
C6-C5-H5	125.9	H33A-C33-H33B	107.8
Ru1-C5-H5	121.0	C35-C34-C39	118.6(5)
C7-C6-C5	107.4(6)	C35-C34-C33	119.6(5)
C7-C6-Ru1	72.6(4)	C39-C34-C33	121.8(6)
C5-C6-Ru1	69.5(3)	C34-C35-C36	120.3(6)
C7-C6-H6	126.3	C34-C35-H35	119.8
C5-C6-H6	126.3	C36-C35-H35	119.8
Ru1-C6-H6	123.3	C37-C36-C35	120.6(6)
C8-C7-C6	110.2(6)	C37-C36-H36	119.7
C8-C7-Ru1	72.0(4)	C35-C36-H36	119.7
C6-C7-Ru1	71.4(4)	C38-C37-C36	119.5(6)
C8-C7-H7	124.9	C38-C37-H37	120.3
C6-C7-H7	124.9	C36-C37-H37	120.3
Ru1-C7-H7	123.2	C37-C38-C39	121.0(6)
C7-C8-C9	107.2(6)	C37-C38-H38	119.5
C7-C8-Ru1	72.1(4)	C39-C38-H38	119.5
C9-C8-Ru1	69.2(3)	C34-C39-C38	119.9(6)
C7-C8-H8	126.4	C34-C39-H39	120.1
C9-C8-H8	126.4	C38-C39-H39	120.1
Ru1-C8-H8	123.9	F4-P3-F1	91.1(3)
C5-C9-C8	107.2(6)	F4-P3-F2	179.9(3)
C5-C9-Ru1	70.9(3)	F1-P3-F2	89.0(2)
C8-C9-Ru1	73.1(3)	F4-P3-F5	91.0(2)
C5-C9-H9	126.4	F1-P3-F5	90.1(2)
C8-C9-H9	126.4	F2-P3-F5	88.8(2)
Ru1-C9-H9	121.4	F4-P3-F6	89.7(2)
N2-C10-P1	110.3(3)	F1-P3-F6	90.1(2)

N2-C10-H10A	109.6	F2-P3-F6	90.4(2)
P1-C10-H10A	109.6	F5-P3-F6	179.2(2)
N2-C10-H10B	109.6	F4-P3-F3	91.0(3)
P1-C10-H10B	109.6	F1-P3-F3	177.7(3)
H10A-C10-H10B	108.1	F2-P3-F3	88.9(2)
N2-C11-P2	112.2(4)	F5-P3-F3	90.8(2)
N2-C11-H11A	109.2	F6-P3-F3	89.0(2)
P2-C11-H11A	109.2		

Table S4. Torsion Angles for **4**

C4-N1-C1-C2	37.3(6)	Ru1-P1-C14-C15	-82.7(5)
Ru1-N1-C1-C2	166.8(4)	C19-C14-C15-C16	-0.2(9)
N1-C1-C2-C3	-34.9(6)	P1-C14-C15-C16	175.9(5)
C1-C2-C3-C4	18.9(7)	C14-C15-C16-C17	1.3(9)
C1-N1-C4-C3	-24.7(6)	C15-C16-C17-C18	-2.1(9)
Ru1-N1-C4-C3	-154.8(4)	C16-C17-C18-C19	1.9(9)
C2-C3-C4-N1	3.0(7)	C17-C18-C19-C14	-0.9(9)
C9-C5-C6-C7	0.5(7)	C15-C14-C19-C18	0.0(9)
Ru1-C5-C6-C7	-63.1(4)	P1-C14-C19-C18	-176.0(4)
C9-C5-C6-Ru1	63.6(4)	C13-P2-C20-C21	119.0(5)
C5-C6-C7-C8	-0.9(7)	C11-P2-C20-C21	-137.2(5)
Ru1-C6-C7-C8	-62.0(4)	Ru1-P2-C20-C21	-14.1(5)
C5-C6-C7-Ru1	61.1(4)	C13-P2-C20-C25	-60.7(5)
C6-C7-C8-C9	0.9(7)	C11-P2-C20-C25	43.1(5)
Ru1-C7-C8-C9	-60.7(4)	Ru1-P2-C20-C25	166.2(4)
C6-C7-C8-Ru1	61.6(4)	C25-C20-C21-C22	-1.3(9)
C6-C5-C9-C8	0.1(7)	P2-C20-C21-C22	179.0(5)
Ru1-C5-C9-C8	64.6(4)	C20-C21-C22-C23	0.0(10)
C6-C5-C9-Ru1	-64.5(4)	C21-C22-C23-C24	1.1(10)
C7-C8-C9-C5	-0.6(7)	C22-C23-C24-C25	-1.0(9)
Ru1-C8-C9-C5	-63.1(4)	C21-C20-C25-C24	1.4(8)
C7-C8-C9-Ru1	62.5(4)	P2-C20-C25-C24	-178.9(4)
C11-N2-C10-P1	68.7(5)	C23-C24-C25-C20	-0.3(8)
C26-N2-C10-P1	-167.0(4)	C11-N2-C26-C27	-161.1(5)
C14-P1-C10-N2	159.4(4)	C10-N2-C26-C27	72.3(6)
C12-P1-C10-N2	50.8(4)	N2-C26-C27-C32	-122.4(6)
Ru1-P1-C10-N2	-74.1(4)	N2-C26-C27-C28	59.3(7)
C10-N2-C11-P2	-68.6(5)	C32-C27-C28-C29	0.4(9)
C26-N2-C11-P2	167.1(4)	C26-C27-C28-C29	178.7(6)
C20-P2-C11-N2	-158.3(4)	C27-C28-C29-C30	-1.1(10)
C13-P2-C11-N2	-52.2(4)	C28-C29-C30-C31	0.4(10)
Ru1-P2-C11-N2	71.7(4)	C29-C30-C31-C32	1.0(10)
C13-N3-C12-P1	65.0(5)	C30-C31-C32-C27	-1.8(10)
C33-N3-C12-P1	-172.4(4)	C28-C27-C32-C31	1.0(9)
C14-P1-C12-N3	139.5(4)	C26-C27-C32-C31	-177.3(6)

C10-P1-C12-N3	-113.6(4)	C13-N3-C33-C34	-69.2(6)
Ru1-P1-C12-N3	7.8(5)	C12-N3-C33-C34	165.5(5)
C12-N3-C13-P2	-62.9(6)	N3-C33-C34-C35	-63.5(7)
C33-N3-C13-P2	175.0(4)	N3-C33-C34-C39	115.5(6)
C20-P2-C13-N3	-147.6(4)	C39-C34-C35-C36	0.6(9)
C11-P2-C13-N3	108.8(4)	C33-C34-C35-C36	179.7(5)
Ru1-P2-C13-N3	-11.6(5)	C34-C35-C36-C37	1.5(9)
C10-P1-C14-C19	-143.2(5)	C35-C36-C37-C38	-0.8(10)
C12-P1-C14-C19	-38.7(6)	C36-C37-C38-C39	-2.0(11)
Ru1-P1-C14-C19	93.2(5)	C35-C34-C39-C38	-3.3(9)
C10-P1-C14-C15	40.9(5)	C33-C34-C39-C38	177.6(6)
C12-P1-C14-C15	145.4(5)	C37-C38-C39-C34	4.1(11)

Table S5. Potential Hydrogen Bonds for **4**

Hydrogen Bond	D—H (Å)	H···A (Å)	D···A (Å)	D—H···A (°)
N1-H1···N3	1.00	2.06	2.953(7)	147.6
C12-H12B···F1[1]	0.99	2.56	3.356(7)	137.5
C15-H15···F6[2]	0.95	2.51	3.454(7)	171.2
C19-H19···F1[1]	0.95	2.47	3.420(6)	175.8
C19-H19···F2[1]	0.95	2.61	3.254(6)	125.0
C25-H25···F5[3]	0.95	2.62	3.566(8)	175.4
C33-H33A···F1[1]	0.99	2.50	3.269(7)	134.7

IV – IR Spectra

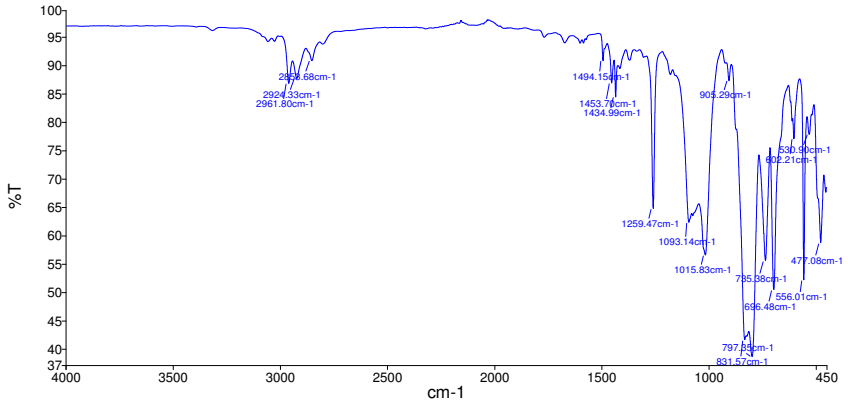

Figure S27. A solid IR spectrum of complex **3** collected with a PerkinElmer UATR Two FT-IR Spectrum Two

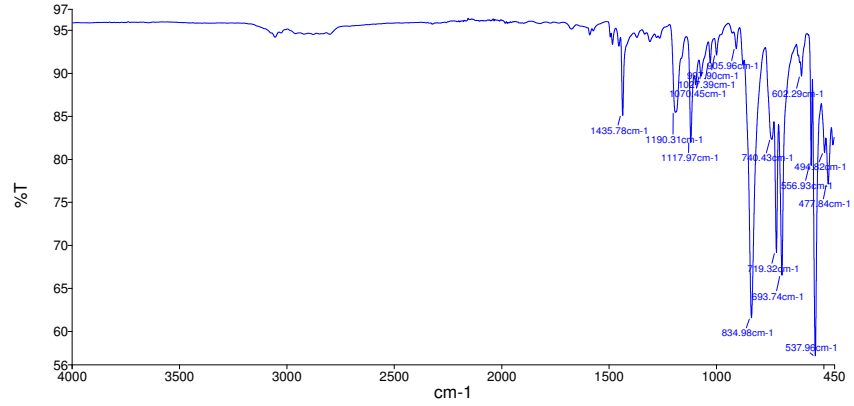

Figure S28. A solid IR spectrum of complex **4** collected with a PerkinElmer UATR Two FT-IR Spectrum Two

V – MALDI Mass Spectrometry Data

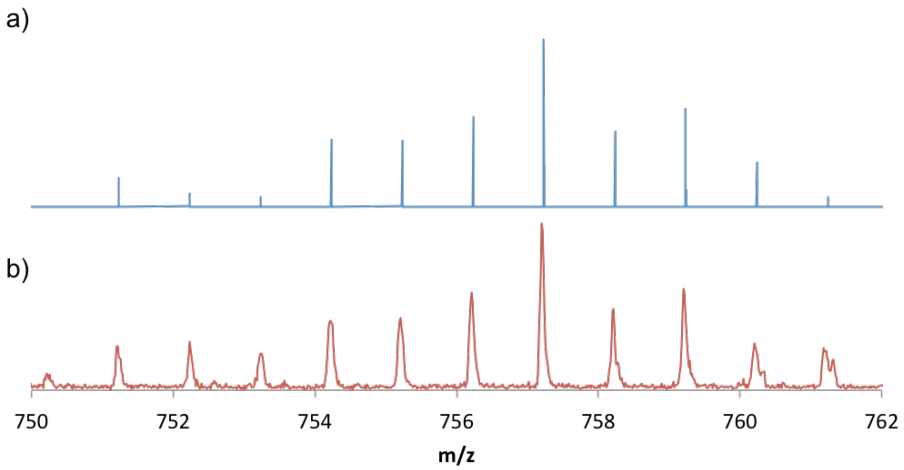

Figure S29. a) Simulation[6] of the mass spectrometry signal for $[\mathbf{3} - PF_6 + H)]^+$. b) Zoom-in of MALDI-TOF mass spectrometry analysis of **3** with pyrene as the matrix.

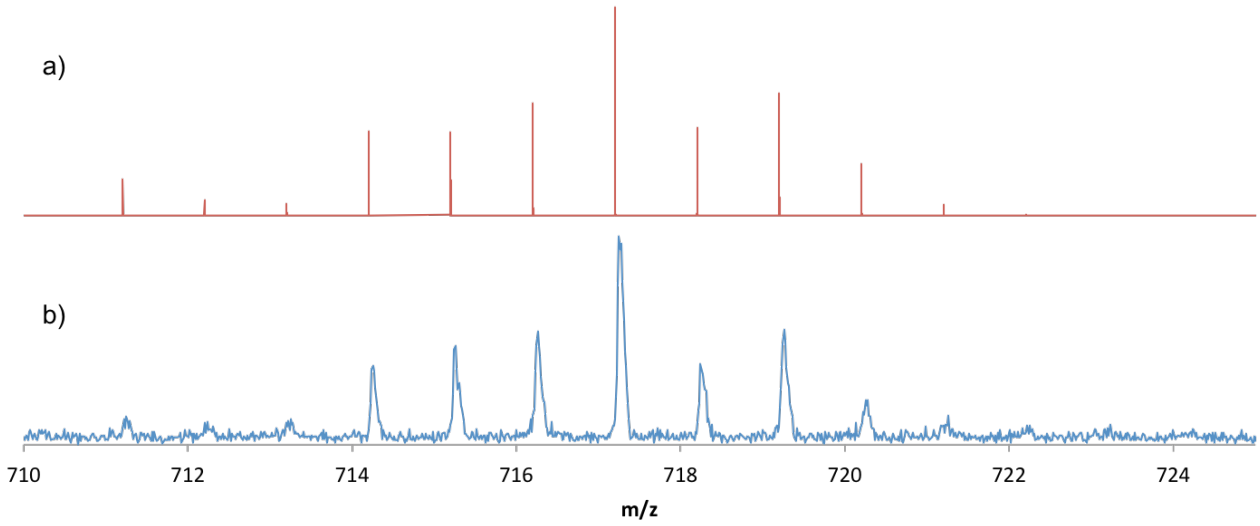

Figure S30. a) Simulation[6] of the mass spectrometry analysis for $[\mathbf{4} - PF_6 - 3H]^{+\bullet}$. b) Zoom-in of MALDI-TOF mass spectrometry analysis of **4** with anthracene as the matrix.

VI – References

1. Bruker-Nonius; SAINT; version; 2012.12, **2012**, Bruker-Nonius, Madison, WI 53711, USA
2. Bruker-Nonius; SADABS; version; 2012.1, **2012**, Bruker-Nonius, Madison, WI 53711, USA.
3. Sheldrick, G., *Acta Crystallogr. Sect. A* **2015,** *A71*, 3-8.
4. Sheldrick, G., *Acta Crystallogr. Sect. C* **2015,** *C71*, 3-8.
5. Gabe, E. J.; Le Page, Y.; Charland, J. P.; Lee, F. L.; White, P. S., *J. Appl. Crystallogr.* **1989,** *22*, 384-387.
6. Patiny, L.; Borel, A., *J. Chem. Inf. Model.* **2013,** *53*, 1223-1228.